Evaluation of MR markers that predict survival in patients with newly diagnosed GBM prior to adjuvant therapy

Suja Saraswathy,
Department of Radiology and Biomedical Imaging, UCSF, Box 2532, Byers Hall, 1700 4th Street, San Francisco, CA 94143-2532, USA

Forrest W. Crawford,
Department of Radiology and Biomedical Imaging, UCSF, Box 2532, Byers Hall, 1700 4th Street, San Francisco, CA 94143-2532, USA

Kathleen R. Lamborn,
Department of Neurological Surgery, UCSF, San Francisco, CA, USA

Andrea Pirzkal,
Department of Radiation Oncology, UCSF, San Francisco, CA, USA

Susan Chang,
Department of Neurological Surgery, UCSF, San Francisco, CA, USA

Soonmee Cha, and
Department of Radiology and Biomedical Imaging, UCSF, Box 2532, Byers Hall, 1700 4th Street, San Francisco, CA 94143-2532, USA

Sarah J. Nelson
Department of Radiology and Biomedical Imaging, UCSF, Box 2532, Byers Hall, 1700 4th Street, San Francisco, CA 94143-2532, USA

UCSF/UCB Joint Graduate Group in Bioengineering, UCSF, San Francisco, CA, USA

Sarah J. Nelson: sarah.nelson@radiology.ucsf.edu

Abstract

Purpose—Glioblastoma Multiforme (GBM) is the most common and lethal primary brain tumor in adults. The goal of this study was to test the predictive value of MR parameters in relation to the survival of patients with newly diagnosed GBM who were scanned prior to receiving adjuvant radiation and chemotherapy.

Methods—The study population comprised 68 patients who had surgical resection and were to be treated with fractionated external beam radiation therapy and chemotherapy. Imaging scans included anatomical MRI, diffusion and perfusion weighted imaging and ^{1}H MRSI. The MR data were acquired 3–5 weeks after surgery and approximately 1 week before treatment with radiation therapy. The diffusion, perfusion and spectroscopic parameter values were quantified and subjected to proportional hazards analysis that was adjusted for age and scanner field strength.

Results—The patients with larger lesion burden based upon volumes of anatomic lesions, volume of CNI2 (number of voxels within the T2 lesion having choline to NAA index >2),

volume of CBV3 (number of pixels within the T2 lesion having relative cerebral blood volume >3), and volume of nADC1.5 (number of pixels within the T2 lesion having normalized apparent diffusion coefficient <1.5) had a higher risk for poor outcome. High intensities of combined measures of lactate and lipid in the T2 and CNI2 regions were also associated with poor survival.

Conclusions—Our study indicated that several pre-treatment anatomic, physiological and metabolic MR parameters are predictive of survival. This information may be important for stratifying patients to specific treatment protocols and for planning focal therapy.

Keywords

Magnetic resonance imaging; Brain tumor; Survival analysis

Introduction

Glioblastoma multiforme (GBM) is the most common and lethal primary brain tumor in adults. It is nearly uniformly fatal, with a median survival of approximately 1 year, despite multimodality treatment approaches. There is considerable heterogeneity in outcome between different patients, with a wide range of survival times. Efforts to understand why some patients live longer than others are expected to provide insights into designing treatment methodologies tailored to individual patients. More accurate assessment of the baseline risk for each patient would allow improved treatment selection and may be valuable for stratifying participants in clinical trials into subgroups with more uniform outcomes.

There are several prognostic factors described in the literature that have been proposed as influencing the survival of patients with glioblastoma multiforme (GBM). These include age, performance status, histological factors, lesion location, extent of surgical resection, adequate radiation therapy, presence of epidermal growth factor, microvessel density, presence of seizures and glucocortical dependency [4,10,12,17,18,27,35,49,57]. While these are of interest for patient evaluation and are being studied in ongoing large scale clinical trials, it would be beneficial if there were more specific, non-invasive parameters for assessing the likelihood of responding to therapy and for evaluating treatment effects in individual patients.

Perfusion weighted MRI has been proposed as a candidate for predicting outcome in patients with glioma. The data obtained with this technique can be used to calculate relative cerebral blood volume (rCBV), which is associated with tumor microvascularity and may be able to distinguish residual and/or recurrent tumor from treatment induced necrosis [7,13,16,19,26,42]. A second technique of interest is diffusion weighted MRI [3]. This reflects the degree of tissue structure, water content, and intra- and extra cellular space and has been proposed as a measure of tumor cellularity [8,9,32,41,51]. A third technique is proton MR spectroscopic imaging (^{1}H MRSI), which enables the quantitative assessment of the spatial distribution of tissue metabolites such as choline, creatine, *N*-acetylaspartate (NAA), lactate, and lipid [39,55].

The current study is based upon the hypothesis that perfusion weighted MRI, diffusion weighted MRI and ^{1}H MRSI are valuable for identifying the true spatial extent and malignancy of tumor and that they are useful for predicting survival in patients with GBM. The objective was to test the prognostic value of these techniques in relation to the survival of patients with newly diagnosed GBM who were scanned after surgical resection but prior to receiving adjuvant radiation and chemotherapy.

Materials and methods

Patient population

The study population comprised 68 patients who had been classified as having grade IV glioma (GBM) based upon histological analysis of tissue samples according to the world health organization (WHO II) criteria. These patients had undergone surgical resection and were to be treated with fractionated external beam radiation therapy (XRT) and chemotherapy. All subjects gave their written informed consent.

MRI examination

MR data were acquired using either 1.5T or 3T MR scanners (GE Healthcare, Milwaukee, WI) using commercially available head coils. Thirty-five of them were scanned with a 1.5T scanner and 33 were scanned with a 3T scanner. All 68 patients had anatomical MRI; 61 patients had perfusion weighted imaging, 65 patients had diffusion weighted imaging and 67 patients had ^{1}H MRSI. The median time between surgery and the pre-radiation scan was 27 days.

Anatomical MRI

The MRI protocol consisted of T1-weighted (TR/TE = 400/12 ms) sagittal scout images; axial (FLAIR) fluid attenuated inversion recovery images (TR/TE/T1 = 1000/143/2200 ms, $220 \times 220 \times 160$ mm^3 field of view (FOV) with $256 \times 256 \times 32$ matrix); and pre- and post contrast T1-weighted (SPGR) spoiled gradient echo images (TR/TE = 32/8, 40 flip angle, $180 \times 240 \times 186$ mm^3 FOV with $192 \times 256 \times 124$ matrix). The FLAIR and pre gadolinium SPGR images were aligned to the post gadolinium SPGR images using software developed in our laboratory [37]. Figure 1 shows examples of FLAIR and T1 weighted post Gadolinium images.

Perfusion weighted imaging

A bolus of 0.1 mmol/kg of body weight gadolinium diethyl enetriamine-pentacid (Gd-DTPA) was injected rapidly into the antecubital vein using an automatic injector (Medrad, Pittsburgh, PA) at a rate of about 5 ml/s. Dynamic susceptibility contrast EPI-gradient echo images were acquired before, during and after the bolus injection. Perfusion weighted imaging parameters were TR/TE of 1500/54 ms, 35° flip angle, 26×26 cm^2 FOV, 128×128 acquisition matrix, 4 mm slice thickness and a total of 80 time points. Perfusion datasets were processed to yield relative cerebral blood volume (rCBV), percent $\Delta R2^*$ recovery, and $\Delta R2^*$ peak height maps using in-house software [30]. Perfusion derived maps were resampled to the same resolution as the SPGR images and rigidly aligned to the SPGR using the VTK software package. Figure 2 shows an example of rCBV and $\Delta R2^*$ peak height maps for one of the patients in the study.

Diffusion weighting imaging

An echo planar imaging (EPI) spin echo (SE) diffusion weighted pulse sequence was used to acquire images that covered supratentorial brain. DWI parameters were TR/TE = 10000/100 ms, matrix $128 \times 128 \times 28$, FOV = 360×360 mm^3, 3 mm slice thickness, b value = 1000 s/mm^2, gradient strength = 0.04 T/m, gradient duration = 21 ms and gradient separation = 27 ms. The apparent diffusion coefficient (ADC) maps were calculated based upon the MR signal intensity decay from diffusion datasets using software developed in-house. Diffusion maps were resampled to the same resolution as the SPGR images and rigidly aligned to them using the VTK software package. Figure 1c shows an example of a diffusionmap for one of the patients in the study.

^{1}H MRSI

Three-dimensional ^{1}H MRSI data (TR/TE = 1000/144 ms, phase encoding matrix = $12 \times 12 \times 8$ or $16 \times 8 \times 8$) with 1 cc nominal spatial resolution was acquired with patient resolved spectroscopic (PRESS) volume localization and very selective saturation (VSS) bands [53] for outer voxel suppression. The post gadolinium T1 weighted SPGR images were used to prescribe the PRESS selected volume to cover both the lesion and 200–300 cc of adjacent normal appearing tissue. Areas of subcutaneous lipids and regions with rapidly varying magnetic susceptibility were avoided whenever possible. Of the patients who received spectroscopy, 35 received lactate-edited spectroscopy as described previously [48]. Figure 3 shows examples of spectra that were obtained from one of the patients using a 1.5T MR scanner with a lactate edited pulse sequence.

The ^{1}H MRSI processing algorithms were developed in-house and have been applied to a large number of patients [36,38]. Briefly, the data were filtered with a Lorentzian function and Fourier transformed, resulting in an array of spectra. The spectra were corrected for baseline variations, phase shifts and frequency shifts within the region of each peak, employing a priori information about the relative location of each metabolite peak. An automatic search procedure was used to identify each resonance. The peak heights of choline, creatine, NAA, lactate and lipid resonances were quantified. In order that the patients who did not have lactate edited ^{1}H MRSI could be included in the analysis, an index of combined contributions was defined to be the absolute peak intensity of the combined peak for the non-lactate edited case and the sum of lactate and lipid values where they were available. The choline to NAA index (CNI) was calculated using an automated technique described by [33]. Metabolic maps were resampled with sinc interpolation to the same resolution as the SPGR images. The spectroscopic data was assumed to be in alignment with the post-gadolinium SPGR images since the ^{1}H MRSI examination was acquired shortly afterward.

Post processing of anatomic images

The contrast enhancing lesion (CEL) and necrotic (NEC) regions were contoured on the post Gd SPGR images. The T2 hyperintense region (T2ALL) was contoured on the FLAIR images and was chosen to exclude the resection cavity. The non-enhancing lesion (NEL) was defined as the T2ALL minus the CEL and NEC regions. There was no attempt to distinguish between edema and residual tumor. All tumor region-of-interest segmentation was performed using in-house semi-automated segmentation software [46]. Normal appearing white matter (NAWM) regions were automatically segmented using the FSL segmentation software package (http://www.fmrib.ox.ac.uk/fsl/fast/index.html).

Analysis

The perfusion and diffusion parameter values were analyzed within each of the segmented anatomical regions (NAWM, CEL, T2ALL, NEL and NEC), limiting the region of analysis for the perfusion data to the region covered by the data acquisition. The diffusion-weighted images covered the entire brain permitting an unrestricted analysis. The metabolite values within the CEL were measured by its intersection with the PRESS excitation volume. To analyze the metabolite values, masks of the anatomic regions of interest were re-sampled to match the resolution of the spectral data. Voxels that were predominantly in NAWM, the CEL, the NEC or the NEL, as well voxels that had metabolite values greater than specific thresholds were used to calculate the statistics for the analysis.

Survival was determined from the date of the MR examination prior to radiation therapy. For circumstances where the patient was still alive (18 out of 68), the survival was censored with the date of the last physician visit. Kaplan–Meier survival curves were computed using

standard techniques as described previously [20]. Figure 4a shows the Kaplan–Meier survival curve for the total population. The Cox proportional hazards model was used to evaluate the influence of each of the parameters on survival. The Cox model is a semi-parametric survival analysis tool that assumes a fixed baseline hazard for the population and computes regression coefficients for a set of predictor variables. The Cox regression analysis for each MR modality was adjusted for age because this has been shown to play a role as a prognostic factor in previous studies [5,24] and for scanner field strength.

Results

Patient age ranged from 27 to 78, with a median of 53 years. Age was not significantly correlated with survival in this study ($P = 0.23$). The median overall survival time was 540 days (18 months) with 18 patients censored. From the analysis of the clinical, immediate post-operative scans, 25 of the patients were assessed as having received a Gross Total Resection (GTR), 34 as having a Sub-total Resection (STR) and nine as having received a biopsy only (Bx). For the sub group who received a GTR the median survival was 649 days (22 months) and for the sub-group who received a STR or Bx the survival was 486 days (16 months). Comparison of the Kaplan–Meier curves for these groups based upon the log rank test gave a *P*-value of 0.115 and with the Wilcoxon test gave a *P*-value of 0.060. Proportional hazards analysis that was adjusted for age had a *P*-value of 0.086.

Anatomic volumes

Fifty-five patients had Gadolinium enhancing lesions and 17 patients had regions of necrosis that could be identified on the T1-weighted images. The median volume of the CEL patients was 2.7 cc with a range of 0.2–44.6 cc ($n = 55$) and the median volume of the NEC was 3.06 with a range of 0.1–20.6 cc ($n = 17$). All 68 patients had regions of T2 hyper-intensity, with the median volume of the T2ALL being 24.4 cc with a range of 0.2–106.4 cc and the median volume of the NEL being18.8 cc with a range of 0.2–79.9 cc. There were no significant differences between lesion volumes based upon field strength. Increasing volumes of the anatomic lesions were associated with worse survival, with the T2ALL volume having the lowest *P*-value ($P = 0.0001$), followed by the NEL ($P = 0.003$), the sum of the CEL + NEC ($P = 0.004$) and the CEL alone ($P = 0.016$). Of interest is that the significance for the T2ALL volume was only marginally decreased when the proportional hazards analysis was adjusted for the CEL or CEL + NEC volumes ($P = 0.0005$ and 0.0004, respectively). This may be due to the fact that the volumes of the CEL and T2ALL were correlated ($R = 0.61$, $P < 0.0001$). As seen in Table 1, there was no relationship to survival for the percentages of the T2ALL that were enhancing and/or necrotic. Figure 4b shows Kaplan–Meier curves for populations with T2ALL regions greater than or less than the median volume of 24.4 cc. The median survival for the population with larger T2ALL lesions was 421 days (14 months) compared with 687 days (23 months) for the population with smaller lesions. The difference between the curves is significant based upon both the log rank ($P = 0.009$) and Wilcoxon tests ($P = 0.010$).

Perfusion parameters

To facilitate comparison of parameter values between patients, the CBV and ΔR2* peak height maps were normalized to the median value within NAWM (see Table 2). The ΔR2 recovery was expressed as a percentage of the baseline (pre-bolus) value and so no further normalization was attempted. The median CBV and ΔR2* peak heights within the CEL (1.3 and 1.2) were significantly greater than in NAWM, while the median values in the NEL were equal or slightly reduced compared to NAWM (1.0 and 0.9). The 90th percentile of these parameters showed similar trends. The median ΔR2* recovery was significantly lower in the CEL (77%) than in other regions (83% in NAWM and 81% in the NEL). For data

acquired using the 3T scanner, the median and 10th percentile of the $\Delta R2^*$ recovery were significantly lower in the CEL (73% and 56%) than with the data from the 1.5T scanner (78% and 65%), presumably due to the increased sensitivity to susceptibility effects at the higher field strength.

Although there is no standard threshold for distinguishing regions with abnormal CBV, previous studies have proposed that values greater than three times NAWM (nCBV >3) are considered to be abnormal [30]. Despite the fact that such regions were relatively small with a median volume of 0.6 cc, it was observed that large nCBV volumes were associated with worse survival ($P = 0.039$). Figure 6a shows the normalized CBV histograms within the critical regions of interest for one of the patients. Note that there is considerable overlap in the values between different regions and, although the distributions are different, there are elevated nCBV values in both the CEL and NEL.

Diffusion parameters

The median ADC was increased in all anatomic regions compared to NAWM but the values were similar in the CEL than in the NEL (1.4 vs. 1.3, see Table 3). Figure 6b shows an example of histograms for the normalized ADC within the various regions and illustrates the large overlap between them. The 10th percentiles of ADC showed similar trends to the median values. Based upon the proportional hazards analysis there was no association between the intensities of ADC or nADC in different regions and survival. As with the perfusion parameters, there is no clear cut-off for ADC that distinguishes tumor versus NAWM and edema. Our previous study had indicated that patients with median nADC value within the T2all less than 1.5 may have worse survival [40] and so we used this threshold to define the volume of the T2ALL that had low nADC. The median volume for the current patient population was 12.9 cc and the P-value for the proportional hazard analysis of these volumes was 0.002 (see Table 1). The median and the 10th percentile of the ADC and nADC values within the anatomic regions were not found to be significantly associated with survival.

Metabolic parameters

The levels of choline, creatine and NAA are summarized in Table 4. The median choline was lower in the CEL than the NEL or NAWM (0.79 vs. 0.97 and 1.00). Median levels of creatine and NAA were decreased in all lesion regions and lowest in the CEL region (0.54 and 0.20, respectively). The CNI was increased in all lesion regions with the highest median values in the overall population being in the CEL region but the highest maximum and sum of CNI value being within the voxels with CNI >2. The histograms in Fig. 6c shows an example of a patient who had highly elevated CNI in the NEL region.

The region of the lesion covered by the intersection of T2ALL and the PRESS selected volume with CNI value greater than 2 (termed the CNI2T) was evaluated as a measure of tumor burden. In this case the number of voxels in the CNI2T region had a median value of 15.9, which means that it was larger than the CEL, but still relatively small compared with the T2ALL. Large CNI2T volumes were associated with poor survival ($P = 0.005$). To see whether this could be attributed merely to a larger CEL region, the survival analysis was repeated with the volume of the CEL and the volume of the CEL + NEC being considered as co-variates. The hazard ratio remained similar and the significance of the CNI2T volumes were $P = 0.021$ and $P = 0.009$. Clearly the metabolic and anatomic parameters provide information about different aspects of the tumor. Figure 5 shows spectral data from in a patient with what was classified as a GTR in the immediate post-surgery scan and had very little contrast enhancement in the pre-RT scan but had highly elevated choline and decreased NAA in the NEL.

It should be noted that there were voxels outside the T2ALL with CNI greater than 2 for many patients (the median total number of voxels with CNI >2 was 30.6 compared with a median number in the CNI2T region of 15.9). From examination of the data it was observed that many of these voxels had relatively normal levels of choline but substantially decreased NAA. The *P*-value for the proportional hazards analysis for the total number of voxels with CNI >2 was 0.059 compared with the *P*-value of 0.005 for those that were within the T2ALL.

Table 5 shows the lactate and lipid levels, which were normalized to the median value of NAA within NAWM in order to facilitate comparisons between patients. In the overall patient population it was observed that although the combined lactate and lipid resonances (nLL) were increased in all lesion regions, they tended to have higher median intensity in the CEL region compared to NAWM (0.23 vs. 0.07). There were however, voxels with high nLL outside the CEL, as indicated by the maximum and the sum of these values, which were highest in the region with voxels having CNI >2. The median number of voxels with elevated nLL was significantly larger for the patients whose data were acquired on a 3T scanner, presumably because the SNR was larger for these patients (median of 18 voxels versus nine voxels for data from 1.5T). When controlling for age and scanner type the proportional hazards analysis indicated that the number of voxels with elevated nLL had a *P*-value of 0.009. Although the volumes were larger, the magnitude of the median, maximum and sum of the nLL values were significantly lower at 3T compared to 1.5T for all regions except for the CEL. Table 5 shows that, when controlling for scanner and age, parameters describing of the intensities of nLL in voxels in the T2ALL and CNI2 were also associated with survival, with the *P*-values for sum of nLL values in T2ALL and CNI2 being the smallest (0.001 and 0.006, respectively).

For the 35 patients who were scanned with lactate edited MRSI it was possible to examine the effects of lactate and lipid separately. An example of lactate edited MRSI spectra is shown in Fig. 3. This demonstrates that there were some voxels within the CEL that have CNI >2 but no lactate and lipid, while other voxels have both CNI >2 and elevated lactate and lipid. The histograms of lactate intensities in Fig. 6d from another of the patients in the study show that there were also voxels with elevated lactate in both the CEL and NEL. The summary values in Table 5 indicate that there were voxels with elevated Lac in all of the regions considered, but that lipid values were more likely to be focused in the CEL. Although none of the lipid parameters were associated with survival, the maximum values of lactate in the T2ALL, CNI2T and CNI2 regions had *P*-values from the proportional hazards analysis of 0.002, 0.008 and 0.0005, respectively. The corresponding summed lactate values were also significant but had larger *P*-values (0.021, 0.032 and 0.011).

Discussion

The survival for patients with glioma depends on both the underlying malignancy of the tumor and its ability to respond to treatment. Since both of these are intrinsic properties of tumor cells, the goal of the present study was to examine if there is a relationship between the post-surgery, pre treatment MR parameters and survival. The most notable finding was that all of the post-surgery, pre-radiation measures of the tumor volume including anatomic, perfusion, diffusion and metabolic parameters were associated with survival. Although previous studies have indicated that the extent of surgical resection may be an important factor in predicting survival for gliomas [18,21,22,24,25] this is the first time that data from pre-treatment scans have been analyzed for both the conventional and the more advanced MR imaging modalities. In the following we discuss the implications of these findings in terms of how perfusion, diffusion and spectroscopic data can be interpreted in the context of anatomic images.

Anatomic measures of tumor burden

The fact that the volume of the T2 hyperintensity had the strongest relationship with survival and that this remained highly significant when controlling for the volumes of the Gadolinium enhancing and necrotic lesions, suggests that it was the most reliable anatomic measure of tumor burden for this population. These findings are in marked contrast to those from a related study performed in our laboratory for patients who were scanned prior to their initial surgery [11]. That study found none of the pre-surgery anatomic lesion volumes to be associated with survival. One explanation of the differences between the results at these two time points is the variability in the extent of resection caused by the location of the tumor, which could mean that there is no clear relationship between pre- and post-surgery volumes. A second explanation is that the volume of T2 hyperintensity in the pre-surgery scan is an unreliable measure of tumor burden because it includes substantial contributions from edema. In either case, this study is indicating that removal of portions of the tumor and the associated reduction in mass effect results in the residual volumes of T2 hyperintensity becoming the most accurate measure of tumor burden.

Measures of tumor cellularity/proliferation from the MRSI data

A further implication of the high level of significance for the volume of the T2 hyperintensity is that the non-enhancing portion of the tumor has an impact upon survival and should therefore play a prominent role in evaluating prognosis and directing therapy. Interestingly the number of voxels with elevated CNI that were within the T2 hyperintensity include substantial portions that were non-enhancing and showed a significant relationship to survival. This implies that the CNI lesion, which reflects a combination of tumor cellularity and increased proliferation, may be a more reliable measure of tumor burden than the Gadolinium enhancing lesion and may be important for distinguishing tumor from edema.

This finding is consistent with our previous studies [28,40,43,44], which showed that the regions with the highest CNI were frequently outside the enhancing tumor volume and that there were substantial differences between the spatial extent of morphologic and metabolic lesions. Note that high CNI values reflect both increased choline due to high cell density or proliferative capacity and loss of NAA [33,34,54]. The presence of voxels outside of the T2 hyperintensity with normal choline and decreased NAA may be due to infiltrative tumor or to impairment of neuronal function in regions close to the site of resection. This may explain the stronger association with survival for the number of voxels with elevated CNI within the T2 hyperintensity compared with the total number of voxels with elevated CNI. Future studies should acquire ^{1}H MRSI data at a field strength of 3T to improve the signal to noise ratio of the data [29] and should examine the patterns of tumor progression for patients who have abnormal voxels outside the T2 hyperintensity in order to determine whether the NAA intensities in these voxels recover with time or whether these regions show evidence of tumor growth.

Measures of tumor burden from DWI data

The existence of large regions with ADC values within the T2 region that were less than 1.5 times normal appearing white matter was observed to be associated with poor survival at pre-surgery [11] and pre-radiation time points. The latter is consistent with previous results from our laboratory in a smaller population of patients [40] and with observations that have linked low ADC with high tumor cellularity [14,23,51,52]. Of interest is that despite the significance of the volumes of lower ADC, there was no relationship between the intensities of ADC in the Gadolinium enhancing volume as had been the case for the data from our pre-surgery population. This may be due to ambiguities in ADC intensity that are induced by post-surgery ischemia in regions close to the surgical cavity and which have been shown to

lead to subsequent regions of Gadolinium enhancement that turn into cystic encephalomalacia in a period of 2–6 months after surgery [47]. Despite this effect, our study implies that the pre-radiation ADC maps may be valuable for assessing the spatial extent of the region of tumor, which is important for defining the target for focal therapy and customizing treatment planning. Other recent reports have indicated that early changes in ADC have a strong potential as an early biomarker for treatment response [9,15].

Measures of tumor burden from PWI data

The presence of regions with increased and abnormal blood vessels is an important characteristic for distinguishing high grade from low grade glioma [6], and is therefore expected to be associated with poor survival. The relationship of the volume of the region within the T2 hyperintensity with CBV greater than three times normal appearing white matter to survival in our post-surgery pre-radiation population is therefore not surprising. It should be noted, however, that the regions with high CBV and high $\Delta R2*$ peak height were relatively small and were located mainly within areas of residual Gadolinium enhancement. The findings in this study are thus consistent with the surgery removing not only a substantial part of the enhancing lesion, but also the major component of the region with abnormal vascular parameters. While the areas with abnormal vascularity are likely to grow larger as the tumor progresses, none of the intensities of the perfusion parameters within the pre-radiation abnormalities were predictive of survival. The comparison of 1.5T and 3T data showed similar qualitative results for the two datasets but gave improved sensitivity for several of the resulting MR parameters [31]. This suggests that 3T should be the field strength used for future studies on patients with brain tumors. The increased sensitivity of the 3T data to vessel permeability as reflected by differences in $\Delta R2*$ recovery between the two field strengths suggest that future studies wishing to measure this parameter would benefit from being performed at the higher field strength.

^{1}H MRSI parameters reflecting malignant behavior

In this study, the number of voxels in the T2 hyperintensity and regions with CNI greater than 2 that had elevated combined levels of lactate and lipid values were also related to poor survival. From the analysis of the lactate edited data it appears that lactate was the key factor contributing to this poor outcome. Increased lactate may occur when the anaerobic glycolic pathway exceeds the capacity of the lactate catabolizing respiratory pathways or when the cellular capacity for exporting lactate to the blood stream is impaired [45,56]. This would indicate tumor metabolism, infiltration and growth. Another possibility is that the lactate peaks are indicators of hypoxia, which has been shown to be a factor in poor response to the treatment of radio or chemotherapy [1]. Underlying mechanisms include the presence of oxygen which is required for fixation of radiation induced damage in DNA, the involvement of hypoxia driving genetic instability and resulting in tumor progression [50]. Previous studies have supported the role of lactate and lipid in defining malignant behavior [2,28].

Conclusion

This study has examined the value of pre-XRT in vivo MR parameters in predicting survival for patients with GBM. Anatomic, physiological and metabolic measures of residual tumor volume were strongly related with survival. Of particular interest is that several of these parameters were different from the factors that were prognostic prior to surgical resection. Factors highlighted in this pre-radiation scan were the contribution of the non-enhancing portion of the T2 hyperintenisty, as well as the role of DWI and ^{1}H MRSI in defining tumor within these regions. While our current study was limited by having incomplete coverage of the T2 lesion for some of the MRSI and PWI datasets, future advances in data acquisition methods are expected to significantly improved coverage and allow these variables to be

used for planning focal therapy. The comparison of 1.5T and 3T data showed similar qualitative results for the two datasets but gave improved sensitivity for several of the resulting MR parameters. This suggests that 3T should be the field strength used for future studies on patients with brain tumors. Other key parameters in predicting outcome were the spatial extent and intensities of the combined lactate and lipid peaks. Results obtained from the lactate-edited ^{1}H MRSI data suggested it is the lactate within non-enhancing tumor that is more relevant in predicting survival than residual lipid. Future studies should investigate the parameters that have been identified in larger populations of patients and see whether they can also be used to assess prognosis at other time points. These results will assist oncologists to interpret the results of MR imaging examinations in order to stratify patients for clinical trials and tailor treatment to each individual tumor.

Acknowledgments

References

1. Aboagye EO, Kelson AB, Tracy M, Workman P. Preclinical development and current status of the fluorinated 2-nitroimidazole hypoxia probe *N*-(2-hydroxy-3,3,3-trifluoropropyl)-2-(2-nitro-1-imidazolyl) acetamide (SR 4554, CRC 94/17): a non-invasive diagnostic probe for the measurement of tumor hypoxia by magnetic resonance spectroscopy and imaging, and by positron emission tomography. Anticancer Drug Des 1998;13:703–730. [PubMed: 9755726]

2. Alger JR, Frank JA, Bizzi A, Fulham MJ, DeSouza BX, Duhaney MO, et al. Metabolism of human gliomas: assessment with H-1 MR spectroscopy and F-18 flourodeoxyglucose PET. Radiology 1990;177:633–641. [PubMed: 2243962]

3. Basser PJ, Pierpaoli C. Microstructural and physiological features of tissues elucidated by quantitative-diffusion-tensor MRI. J Magn Reson B 1996;111:209–219. doi:10.1006/jmrb.1996.0086. [PubMed: 8661285]

4. Burger PC, Green SB. Patient age, histologic features, and length of survival in patients with glioblastoma multiforme. Cancer 1987;59:1617–1625. doi:10.1002/1097-0142(19870501)59:9<1617::AID-CNCR2820590916>3.0.CO;2-X. [PubMed: 3030531]

5. Burger PC, Vogel FS, Green SB, Strike TA. Glioblastoma multiforme and anaplastic astrocytoma. Pathologic criteria and prognostic implications. Cancer 1985;56:1106–1111. doi:10.1002/1097-0142(19850901)56:5<1106::AID-CNCR2820560525>3.0.CO;2-2. [PubMed: 2990664]

6. Catalaa I, Henry R, Dillon WP, Graves EE, McKnight TR, Lu Y, et al. Perfusion, diffusion and spectroscopy values in newly diagnosed cerebral gliomas. NMR Biomed 2006;19:463–475. doi:10.1002/nbm.1059. [PubMed: 16763973]

7. Cha S, Lupo JM, Chen MH, Lamborn KR, McDermott MW, Berger MS, et al. Differentiation of glioblastoma multiforme and single brain metastasis by peak height and percentage of signal intensity recovery derived from dynamic susceptibility-weighted contrast-enhanced perfusion MR imaging. AJNR Am J Neuroradiol 2007;28:1078–1084. doi:10.3174/ajnr.A0484. [PubMed: 17569962]

8. Chang L, Mc Bride D, Miller BL, Cornford M, Booth RA, Buchthal SD, et al. Localized in vivo 1H magnetic resonance spectroscopy and in vitro analyses of heterogeneous brain tumors. J Neuroimaging 1995;5:157–163. [PubMed: 7626823]

9. Chenevert TL, Stegman LD, Taylor JM, Robertson PL, Greenberg HS, Rehemtulla A, et al. Diffusion magnetic resonance imaging: an early surrogate marker of therapeutic efficacy in brain tumors. J Natl Cancer Inst 2000;92:2029–2036. doi:10.1093/jnci/92.24.2029. [PubMed: 11121466]

10. Coffey RJ, Lunsford LD. Factors determining survival of patients with malignant gliomas diagnosed by stereotactic biopsy. Appl Neurophysiol 1987;50:183–187. doi:10.1159/000100707. [PubMed: 2835932]

11. Crawford FW, Khayal IS, McGue C, Saraswathy S, Pirzkall A, Cha S, Lamborn KR, Chang SM, Berger MS, Nelson SJ. Relationship of pre-surgery metabolic and physiological MR imaging parameters to survival for patients with untreated GBM. J Neurooncol. 2008 (in press).

12. Etienne MC, Formento JL, Lebrun-Frenay C, Gioanni J, Chatel M, Paquis P, et al. Epidermal growth factor receptor and labeling index are independent prognostic factors in glial tumor outcome. Clin Cancer Res 1998;4:2383–2390. [PubMed: 9796969]

13. Fuss M, Wenz F, Scholdei R, Essig M, Debus J, Knopp MV, et al. Radiation-induced regional cerebral blood volume (rCBV) changes in normal brain and lowgrade astrocytomas: quantification and time and dose-dependent occurrence. Int J Radiat Oncol Biol Phys 2000;48:53–58. doi: 10.1016/S0360-3016(00)00590-3. [PubMed: 10924971]

14. Guo AC, Cummings TJ, Dash RC, Provenzale JM. Lymphomas and high grade astrocytomas: comparison of water diffusibility and histologic characteristics. Radiology 2002;224:177–183. doi: 10.1148/radiol.2241010637. [PubMed: 12091680]

15. Hamstra DA, Chenevert TL, Moffat BA, Johnson TD, Meyer CR, Mukherji SK, et al. Evaluation of the functional diffusion map as an early biomarker of time-to-progression and overall survival in high-grade glioma. Proc Natl Acad Sci USA 2005;102:16759–16764. doi:10.1073/pnas. 0508347102. [PubMed: 16267128]

16. Henry RG, Vigneron DB, Fischbein NJ, Grant PE, Day MR, Noworolski SM, et al. Comparison of relative cerebral blood volume and proton spectroscopy in patients with treated gliomas. AJNR Am J Neuroradiol 2000;21:357–366. [PubMed: 10696024]

17. Hohwieler SM, Freidberg SR, Heatley GJ, Lo TC. Glucocorticoid dependency as a prognostic factor in radiotherapy for cerebral gliomas. Acta Oncol 1989;28:51–55. doi: 10.3109/02841868909111181. [PubMed: 2539846]

18. Jeremic B, Grujicic D, Antunovic V, Djuric L, Stojanovic M, Shibamoto Y. Influence of extent of surgery and tumor location on treatment outcome of patients with glioblastoma multiforme treated with combined modality approach. J Neurooncol 1994;21:177–185. doi:10.1007/BF01052902. [PubMed: 7861194]

19. Johnson G, Wetzel SG, Cha S, Babb J, Tofts PS. Measuring blood volume and vascular transfer constant from dynamic, T(2)*-weighted contrast-enhanced MRI. Magn Reson Med 2004;51:961–968. doi:10.1002/mrm.20049. [PubMed: 15122678]

20. Kaplan EL, Meier P. Nonparametric estimation from incomplete observations. J Am Stat Assoc 1958;53:457–481. doi:10.2307/2281868.

21. Keles GE, Anderson B, Berger MS. The effect of extent of resection on time to tumor progression and survival in patients with glioblastoma multiforme of the cerebral hemisphere. Surg Neurol 1999;52:371–379. doi:10.1016/S0090-3019(99)00103-2. [PubMed: 10555843]

22. Keles GE, Lamborn KR, Chang SM, Prados MD, Berger MS. Volume of residual disease as a predictor of outcome in adult patients with recurrent supratentorial glioblastomas multiforme who are undergoing chemotherapy. J Neurosurg 2004;100:41–46. [PubMed: 14743910]

23. Kono K, Inoue Y, Nakayama K, Shakudo M, Morino M, Ohata K, et al. The role of diffusion-weighted imaging in patients with brain tumors. AJNR Am J Neuroradiol 2001;22:1081–1088. [PubMed: 11415902]

24. Lacroix M, Abi-Said D, Fourney DR, Gokaslan ZL, Shi W, DeMonte F, et al. A multivariate analysis of 416 patients with glioblastoma multiforme: prognosis, extent of resection, and survival. J Neurosurg 2001;95:190–198. [PubMed: 11780887]

25. Lamborn KR, Chang SM, Prados MD. Prognostic factors for survival of patients with glioblastoma: recursive partitioning analysis. Neuro-oncology 2004;6:227–235. doi:10.1215/S1152851703000620. [PubMed: 15279715]

26. Lee MC, Cha S, Chang SM, Nelson SJ. Dynamic susceptibility contrast perfusion imaging of radiation effects in normal-appearing brain tissue: changes in the first-pass and recirculation phases. J Magn Reson Imaging 2005;21:683–693. doi:10.1002/jmri.20298. [PubMed: 15906330]

27. Leon SP, Folkerth RD, Black PM. Microvessel density is a prognostic indicator for patients with astroglial brain tumors. Cancer 1996;77:362–372. doi:10.1002/(SICI)1097-0142(19960115)77:2<362::AID-CNCR20>3.0.CO;2-Z. [PubMed: 8625246]

28. Li X, Jin H, Lu Y, Oh J, Chang S, Nelson SJ. Identification of MRI and 1H MRSI parameters that may predict survival for patients with malignant gliomas. NMR Biomed 2004;17:10–20. doi: 10.1002/nbm.858. [PubMed: 15011246]

29. Li Y, Osorio JA, Ozturk-Isik E, Chen AP, Xu D, Crane JC, et al. Considerations in applying 3D PRESS H-1 brain MRSI with an eight-channel phased-array coil at 3T. Magn Reson Imaging 2006;24:1295–1302. doi:10.1016/j.mri.2006.07.012. [PubMed: 17145400]

30. Lupo JM, Cha S, Chang SM, Nelson SJ. Dynamic susceptibility-weighted perfusion imaging of high-grade gliomas: characterization of spatial heterogeneity. AJNR Am J Neuroradiol 2005;26:1446–1454. [PubMed: 15956514]

31. Lupo JM, Lee MC, Han ET, Cha S, Chang SM, Berger MS, et al. Feasibility of dynamic susceptibility contrast perfusion MR imaging at 3T using a standard quadrature head coil and eight-channel phased-array coil with and without SENSE reconstruction. J Magn Reson Imaging 2006;24:520–529. doi:10.1002/jmri.20673. [PubMed: 16888776]

32. McBride DQ, Miller BL, Nikas DL, Buchthal S, Chang L, Chiang F, et al. Analysis of brain tumors using 1H magnetic resonance spectroscopy. Surg Neurol 1995;44:137–144. doi: 10.1016/0090-3019(95)00139-5. [PubMed: 7502203]

33. McKnight TR, Noworolski SM, Vigneron DB, Nelson SJ. An automated technique for the quantitative assessment of 3D-MRSI data from patients with glioma. J Magn Reson Imaging 2001;13:167–177. doi:10.1002/1522-2586(200102)13:2<167::AID-JMRI1026>3.0.CO;2-K. [PubMed: 11169821]

34. McKnight TR, von dem Bussche MH, Vigneron DB, Lu Y, Berger MS, McDermott MW, et al. Histopathological validation of a three-dimensional magnetic resonance spectroscopy index as a predictor of tumor presence. J Neurosurg 2002;97:794–802. [PubMed: 12405365]

35. Miller PJ, Hassanein RS, Girim PG, Kimler BF, O'Boynick P, Evans RG. Univariate and multivariate statistical analysis of high-grade gliomas: the relationship of radiation dose and other prognostic factors. Int J Radiat Oncol Biol Phys 1990;1:275–280. [PubMed: 2168352]

36. Nelson SJ. Analysis of volume MRI and MR spectroscopic imaging data for the evaluation of patients with brain tumors. Magn Reson Med 2001;46:228–239. doi:10.1002/mrm.1183. [PubMed: 11477625]

37. Nelson SJ, Nalbandian AB, Proctor E, Vigneron DB. Registration of images from sequential MR studies of the brain. J Magn Reson Imaging 1994;4:877–883. doi:10.1002/jmri.1880040621. [PubMed: 7865950]

38. Nelson SJ, Huhn S, Vigneron DB, Day MR, Lawrence LW, Prados M, et al. Volume MRI and MRSI techniques for the quantitation of treatment response in brain tumors: presentation of a detailed case study. J Magn Reson Imaging 1997;7:1146–1152. doi:10.1002/jmri.1880070630. [PubMed: 9400861]

39. Nelson SJ, Vigneron DB, Dillon WP. Serial evaluation of patients with brain tumors using volume MRI and 3D 1H MRSI. NMR Biomed 1999;12:123–138. doi:10.1002/(SICI)1099-1492(199905)12:3<123::AID-NBM541>3.0.CO;2-Y. [PubMed: 10414947]

40. Oh J, Henry RG, Pirzkall A, Lu Y, Li X, Catalaa I, et al. Survival analysis in patients with glioblastoma multiforme: predictive value of choline-to-*N*-acetylaspartate index, apparent diffusion coefficient, and relative cerebral blood volume. J Magn Reson Imaging 2004;19:546–554. doi:10.1002/jmri.20039. [PubMed: 15112303]

41. Peeling J, Sutherland G. High-resolution 1H NMR spectroscopy studies of extracts of human cerebral neoplasms. Magn Reson Med 1992;24:123–136. doi:10.1002/mrm.1910240113. [PubMed: 1556919]

42. Perkio J, Aronen HJ, Kangasmaki A, Liu Y, Karonen K, Salvolainen S, et al. Evaluation of four postprocessing methods for determination of cerebral blood volume and mean transit time by dynamic susceptibility contrast imaging. Magn Reson Med 2002;47:973–981. doi:10.1002/mrm.10126. [PubMed: 11979577]

43. Pirzkall A, McKnight TR, Graves EE, Carol MP, Sneed PK, Wara WW, et al. MR-spectroscopy guided target delineation for high-grade gliomas. Int J Radiat Oncol Biol Phys 2001;50:915–928. doi:10.1016/S0360-3016(01)01548-6. [PubMed: 11429219]

44. Pirzkall A, Li X, Oh J, Chang S, Berger MS, Larson DA, et al. 3D MRSI for resected high-grade gliomas before RT: tumor extent according to metabolic activity in relation to MRI. Int J Radiat Oncol Biol Phys 2004;59:126–137. doi:10.1016/j.ijrobp.2003.08.023. [PubMed: 15093908]

45. Prichard JW. What the clinician can learn from MRS lactate measurement. NMR Biomed 1991;4:99–102. doi:10.1002/nbm.1940040212. [PubMed: 1859788]

46. Saraswathy, S.; Crawford, F.; Nelson, SJ. Semi-automated segmentation of brain tumor lesions in MR Images. Proceedings of 13th ISMRM meeting (abstract); Seattle, WA, USA. 2006.

47. Smith JS, Cha S, Mayo MC, McDermott MW, Parsa AT, Chang SM, et al. Serial diffusion-weighted magnetic resonance imaging in cases of glioma: distinguishing tumor recurrence from postresection injury. J Neurosurg 2005;103:428–438. [PubMed: 16235673]

48. Star-Lack J, Spielman D, Adalsteinsson E, Kurhanewicz J, Terris DJ, Vigneron DB. In vivo lactate editing with simultaneous detection of choline, creatine, NAA, and lipid singlets at 1.5T using PRESS excitation with applications to the study of brain and head and neck tumors. J Magn Reson 1998;133:243–254. doi:10.1006/jmre.1998.1458. [PubMed: 9716465]

49. Steltzer KJ, Sauve KI, Spence AM, Griffin TW, Berger MS. Corpus callosum involvement as a prognostic factor for patients with highgrade astrocytoma. Int J Radiat Oncol Biol Phys 1997;38:27–30. doi:10.1016/S0360-3016(96)00632-3. [PubMed: 9212000]

50. Stone, HB.; Brown, JM.; Phillips, TL.; Sutherland, RM. Oxygen in human tumors: correlations between methods of measurement, response to therapy. Summary of a workshop held November 19–20, 1992, at the National Cancer Institute, Bethesda, Maryland; Radiat Res. 1993. p. 422-434.doi:10.2307/3578556

51. Sugahara T, Korogi Y, Kochi M, Ikushima I, Shigematu Y, Hirai T, et al. Usefulness of diffusion weighted MRI with echoplanar technique in the evaluation of cellularity in gliomas. J Magn Reson Imaging 1999;9:53–60. doi:10.1002/(SICI)1522-2586(199901)9:1<53::AID-JMRI7>3.0.CO;2-2. [PubMed: 10030650]

52. Tien RD, Felsberg GJ, Friedman H, Brown M, MacFall J. MR imaging of high-grade cerebral gliomas: value of diffusion-weighted echoplanar pulse sequences. AJR Am J Roentgenol 1994;162:671–677. [PubMed: 8109520]

53. Tran TK, Vigneron DB, Sailasuta N, Tropp J, Le Roux P, Kurhanewicz J, et al. Very selective suppression pulses for clinical MRSI studies of brain and prostate cancer. Magn Reson Med 2000;43:23–33. doi:10.1002/(SICI)1522-2594(200001)43:1<23::AID-MRM4>3.0.CO;2-E. [PubMed: 10642728]

54. Usenius JP, Vaino P, Hernesniemi J, Kauppinen RA. Choline-containing compounds in human astrocytomas studied by 1H NMR spectroscopy in vivo and in vitro. J Neurochem 1994;63:1538–1543. [PubMed: 7931308]

55. Vigneron DB, Bollen A, McDermott M, Wald LL, May MR, Noworolski SM, et al. Three-dimensional magnetic resonance spectroscopic imaging of histologically confirmed brain tumors. Magn Reson Imaging 2001;19:89–101. doi:10.1016/S0730-725X(01)00225-9. [PubMed: 11295350]

56. Warburg, O. The metabolism of tumors. New York: Constable; 1930.

57. Winger MJ, Macdonald DR, Cairncross JG. Supratentorial anaplastic gliomas in adults. The prognostic importance of extent of resection and prior low-grade glioma. J Neurosurg 1989;71:487–493. [PubMed: 2552044]
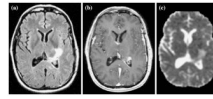
Fig. 1.
Example of a FLAIR image (**a**), a T1 weighted post-contrast image (**b**), and an apparent diffusion coefficient map (**c**) from corresponding slices in a 68 year old patient with a newly diagnosed GBM post surgery and prior to radiation therapy
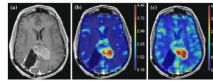
Fig. 2.
Example of a post-contrast T weighted image (**a**) and overlaid perfusion maps showing (**b**) rCBV and (**c**) ΔR2* peak height maps for a patient with a 46 year old patient with GBM
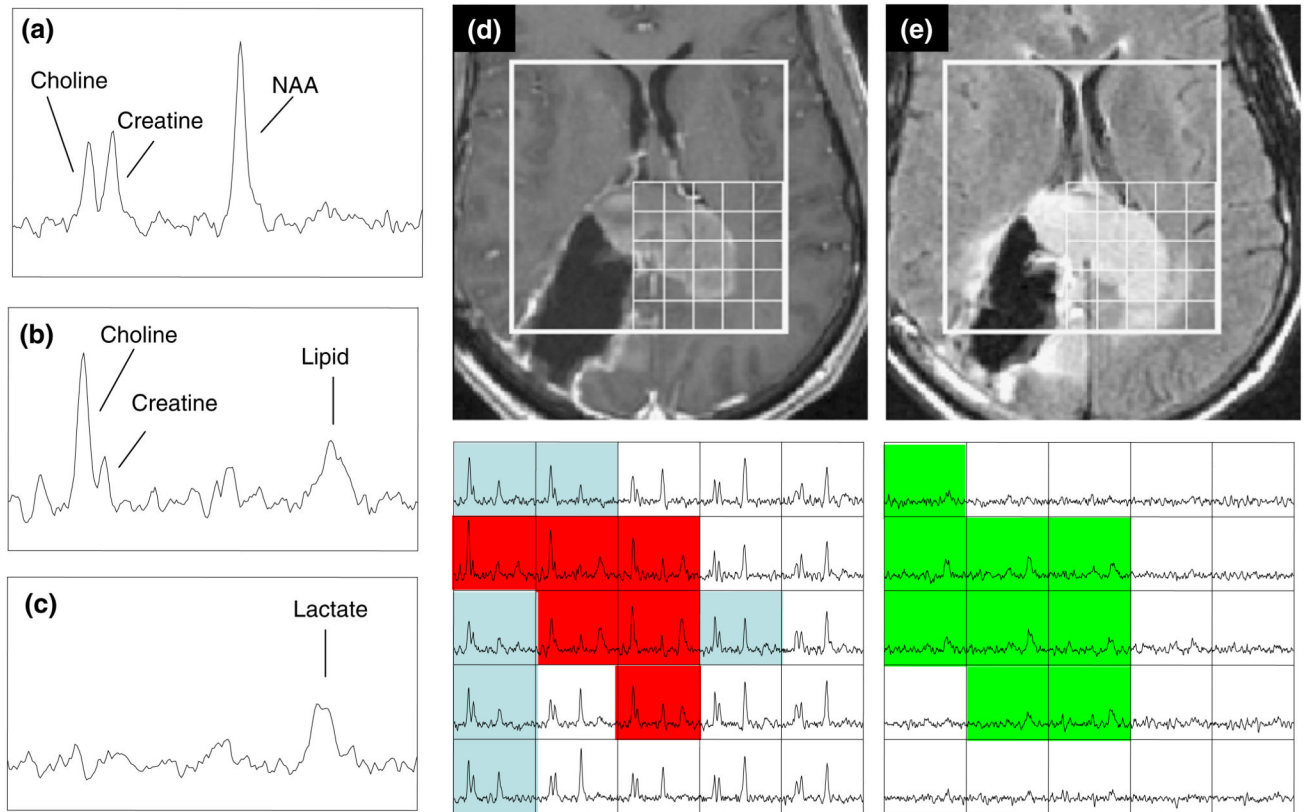
Fig. 3.
Spectra and images from the same patient as in Fig. 2. The individual spectra from normal brain (**a**) shows peaks corresponding to NAA, choline and creatine, from the summed spectra in the tumor (**b**) with an additional peak from lipid, and from the difference spectra in the tumor (**c**) showing the lactate peak. The T1-weighted post-contrast (**d**) and FLAIR (**e**) images display the PRESS selected volume and the corresponding arrays of summed (left) and difference (right) of the lactate-edited spectra. Voxels in the spectral arrays that are highlighted in blue have CNI >2 but no lipid, voxels in red have both CNI >2 and lipid with SNR >6.0 and voxels in green have lactate with SNR >6.0

Fig. 4.
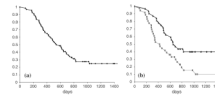Kaplan–Meier survival curves for (**a**) all patients and (**b**) for groups of patients with T2ALL lesion volume greater than (gray line) or less than (black line) the median value
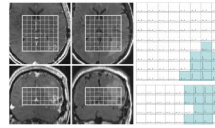
Fig. 5.
T1 post contrast and FLAIR images from a 49 year old patient with a newly diagnosed GBM whose lesion was classified as a gross total resection at the time of surgery. Four weeks later and immediately prior to treatment with radiation small regions of Gadolinium enhancement can be observed in the medial edge of the lesion and a more extensive area of hyperintensity on FLAIR images. The MRSI data show that this abnormality has highly elevated CNI with the blue shading showing voxels in the axial and coronal planes that have abnormal CNI which ranges from 3.2 to 30.7. Note that the level of choline is so high in tumor relative to normal voxels that the intensity scale has to be reduced by a factor of 4 to be able to visualize them within the same array
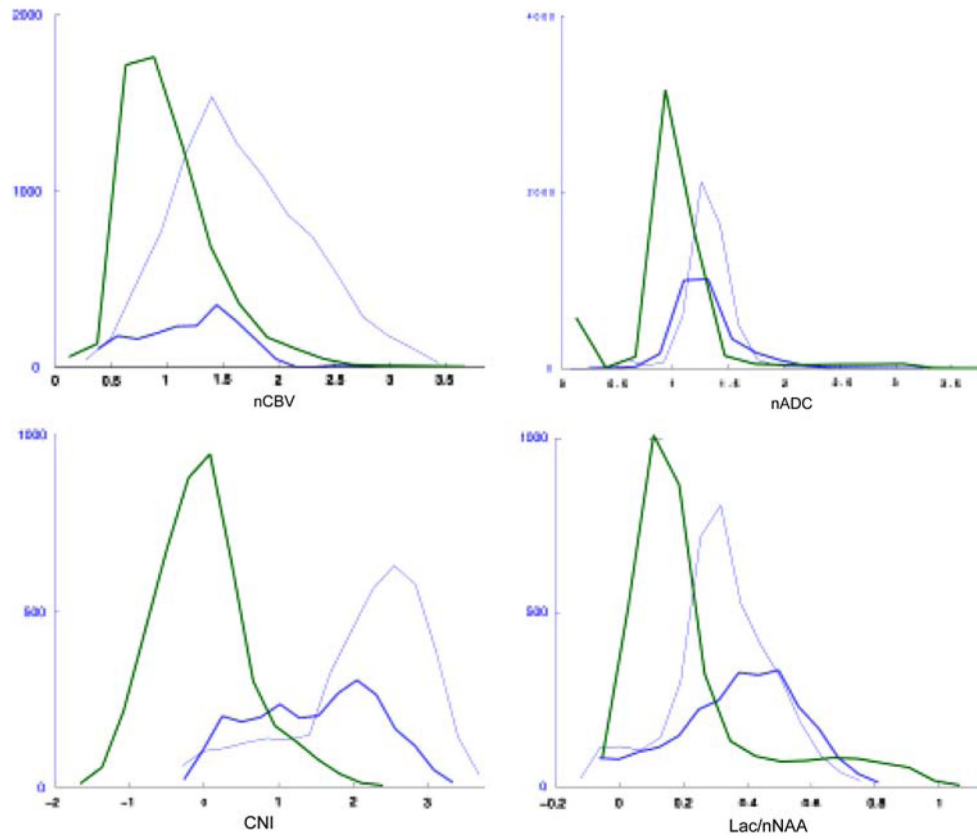
Fig. 6.
Distribution of rCBV, ADC, CNI and Lac/nNAA values in normal appearing white matter
(NAWM—green curves), contrast enhancement lesion (CEL—dark blue curves) and non-
enhancing lesion (NEL—light blue curves) regions for the patient who was shown in Fig. 1

Table 1

Median values of volumes for the CEL, CEL + NEC, NEL and T2ALL, as well as the percentage of each volume in T2ALL for patients where these regions could be identified

Parameter	CEL (*N* = 50)	CEL + NEC (*N* = 50)	NEL (*N* = 68)	T2ALL (*N* = 68)
Total volume (cc)	2.7 ± 5.8	3.8 ± 11.6	14.1 ± 14.3	24.4 ± 15.0
P-value for total volume	0.016*	0.004*	0.003*	0.0001*
Volume within T2ALL (%)	20.1 ± 19.8	21.5 ± 21.2	82.7 ± 21.4	100
P-value for % volume	0.788	0.653	0.672	n/a
Volumes overlapping with T2ALL	nCBV >3 (*N* = 61)	nADC <1.5 (*N* = 65)	snrLL >6 (*N* = 59)	CNI >2 (*N* = 67)
Volume cc/voxels	0.6 ± 2.8	15.4 ± 15.8	17.1 ± 4.9	15.9 ± 4.9
P-value	0.039*	0.006*	0.009*	0.005*

The *P*-values are age and scanner-adjusted Cox regression significance values for survival. The lower panels show similar results for the volumes of physiological and metabolic lesions that were restricted to the voxels in the intersection of the T2ALL and the excitation volume

Table 2

Median and percentiles of values of nCBV from perfusion maps in different regions
($N = 51$ in the CEL, while $N = 61$ for the other regions)

Parameter	NAWM ($N = 61$)	CEL ($N = 51$)	NEL ($N = 61$)	T2ALL ($N = 61$)
nCBV median	1.0	1.3 ± 0.8	1.0 ± 0.4	1.1 ± 0.4
nCBV 90th perc	1.8 ± 0.3	2.2 ± 1.4	2.0 ± 0.8	2.1 ± 1.0
nPH median	1.0	1.2 ± 0.7	0.9 ± 0.4	0.9 ± 0.4
nPH 90th perc	1.7 ± 0.3	1.9 ± 2.3	1.6 ± 0.8	1.8 ± 2.0
%REC median	83 ± 10.4	77 ± 13.5	81 ± 11.4	81 ± 11.8
%REC 10th perc	76 ± 10.5	62 ± 15.7	72 ± 12.4	69 ± 13.6

The median values in CEL and 90% were different from NAWM. The median values in the NEL were not different from NAWM but the 90% has a P-value of 0.014 compared with NAWM. The results were similar for the peak height estimates. The only values that were significantly different between data acquired on the 1.5T and 3T scanners were the recovery values in the CEL. None of these parameters were related to survival based on the proportional hazards analysis

Table 3

Median and 10th percentile values of ADC and normalized ADC in different regions

Parameter	WM	CEL	NEL	T2ALL
ADC median	811 ± 38	1175 ± 301	1089 ± 241	1093 ± 237
ADC 10th percentile	696 ± 63	876 ± 199	838 ± 201	838 ± 199
nADC median	1.0	1.4 ± 0.4	1.3 ± 0.3	1.4 ± 0.3
nADC 10th percentile	0.9 ± 0.1	1.1 ± 0.3	1.0 ± 0.3	1.0 ± 0.3

The values in all of these regions were significantly different from the values in NAWM but not between themselves

Table 4

Median, maximum values and summed values of the spectroscopic metabolite maps in different regions

Parameter	WM (N = 67)	CEL (N = 49)	NEL (N = 67)	T2ALL (N = 67)	CNI2T (N = 67)	CNI2 (N = 67)
nCho median	1.00	0.79 ± 1.04	0.97 ± 0.86	0.90 ± 0.50	1.18 ± 0.49	1.22 ± 0.33
nCho max	1.53 ± 0.54	0.84 ± 1.20	1.38 ± 1.23	1.50 ± 1.21	1.56 ± 1.21	1.81 ± 2.38
nCr median	1.00	0.54 ± 0.52	0.76 ± 0.37	0.70 ± 0.36	0.75 ± 0.29	0.87 ± 0.25
nNAA median	1.00	0.20 ± 0.18	0.41 ± 0.21	0.34 ± 0.18	0.36 ± 0.17	0.49 ± 0.18
CNI median	−0.01 ± 0.41	3.23 ± 4.35	2.78 ± 4.68	2.35 ± 3.57	3.45 ± 1.88	2.77 ± 0.81
CNI max	2.56 ± 3.08	3.43 ± 4.68	4.29 ± 5.67	5.05 ± 5.56	5.79 ± 5.55	5.77 ± 6.03
CNI sum	3.24 ± 20.12	3.42 ± 21.20	15.31 ± 48.19	50.5 ± 94.10	41.59 ± 95.62	78.60 ± 110.50

There was no significant difference between the values at 15T and 3T field strengths. None of these parameters exhibited a significant relationship to survival

Table 5

Median, maximum and sum of nLL = (lactate + lipid)/NAA (*n* = 67) and *P*-values for the proportional hazards analysis with age and scanner field strength being considered as covariates

Parameter	NAWM	CEL	NEL	T2ALL	CNI2T	CNI2
nLL median	0.07 ± 0.08	0.23 ± 0.22	0.12 ± 0.12	0.15 ± 0.18	0.16 ± 0.08	0.11 ± 0.13
				P = 0.015		*P* = 0.027
nLL max	0.21 ± 0.30	0.29 ± 0.38	0.25 ± 0.29	0.34 ± 0.71	0.32 ± 0.71	0.32 ± 0.73
				P = 0.043		*P* = 0.022
nLL sum	2.00 ± 2.92	0.29 ± 2.02	1.03 ± 2.39	1.62 ± 9.22	1.61 ± 10.37	3.27 ± 11.96
				P = 0.001	*P* = 0.010	*P* = 0.006
nLac median	0.07 ± 0.06	0.21 ± 0.20	0.16 ± 0.11	0.17 ± 0.07	0.19 ± 0.07	0.13 ± 0.06
						P = 0.030
nLac max	0.20 ± 0.16	0.21 ± 0.34	0.24 ± 0.18	0.29 ± 0.17	0.30 ± 0.15	0.29 ± 0.18
				P = 0.002	*P* = 0.008	*P* = 0.0005
nLac sum	2.80 ± 1.68	0.20 ± 1.80	0.91 ± 2.18	2.05 ± 4.06	2.28 ± 4.57	3.07 ± 4.72
				P = 0.021	*P* = 0.032	*P* = 0.011
nLip median	0.02 ± 0.07	0.24 ± 0.32	0.06 ± 0.09	0.11 ± 0.08	0.12 ± 0.11	0.05 ± 0.09
nLip max	0.19 ± 0.38	0.24 ± 0.32	0.21 ± 0.28	0.31 ± 0.36	0.31 ± 0.34	0.25 ± 0.32
nLip sum	1.23 ± 1.88	0.24 ± 2.29	0.37 ± 1.88	2.02 ± 4.95	1.23 ± 4.02	1.35 ± 4.13

Significance levels are shown only for the cases where *P* < 0.05. Data acquired using a 1.5T scanner used a lactate edited sequence (*n* = 35) and the values of nLac (Lactate/nNAA) and nLip (Lipid/nNAA) were also available